J Therm Spray Tech
https://doi.org/10.1007/s11666-024-01793-5

ORIGINAL RESEARCH ARTICLE

Study of the Propane Detonation Spraying under Different Gun Structures

Hua-Kang Li[1,2] · Du Wang[2] · Yong-Jing Cui[3] · Wen Lu[1,2] · Jun-Kai Wu[1,2] · Zhi-Min Wang[2,4] · Feng-Ming Chu[1] · Zhen-Yu Tian[2,4,5]

Submitted: 28 December 2023 / in revised form: 9 April 2024 / Accepted: 16 May 2024

Abstract Detonation spraying is a technique that uses the high-temperature, high-velocity detonation waves to deposit the molten metal particles onto the target surface. The effect of the detonation spraying is influenced by the structure of the gun significantly. A series of detonation spraying gun two-dimensional (2-D) numerical models with various spray gun structures (slope lengths from 5 to 45 mm with a step of 10 mm) were established in this work, to investigate the spray performance. During the process of gas detonation, the interaction between the detonation wave and obstacles results in the generation of reflected waves, which exerts an accelerating effect on flame. Simultaneously, collisions between the flame front and obstacles introduce energy losses. Based on the above factors, the following results can be obtained: when the slope length at the nozzle diameter change point is 5 mm, the maximum flow velocity is achieved at the spray gun outlet. When the slope length at the transition point of the spray gun is 25 mm, the maximum temperature is reached at the spray gun outlet. When the slope length at the transition point of the spray gun is 45 mm, the maximum pressure is reached at the spray gun outlet. This work can contribute to the design of the detonation gun.

Keywords detonation spraying · flame acceleration · numerical simulation · spray gun design · variable diameter

✉ Feng-Ming Chu
cfm@mail.buct.edu.cn

✉ Zhen-Yu Tian
tianzhenyu@iet.cn

[1] College of Mechanical and Electrical Engineering, Beijing University of Chemical Technology, Beijing 100029, China

[2] Institute of Engineering Thermophysics, Chinese Academy of Sciences, Beijing 100190, China

[3] AECC Beijing Institute of Aeronautical Materials, Beijing 100095, China

[4] University of the Chinese Academy of Sciences, Beijing 100049, China

[5] State Key Laboratory of Coal Conversion, Institute of Engineering Thermophysics, Chinese Academy of Sciences, Beijing 100190, China

Introduction

Detonation spraying is a type of thermal spraying technology that can produce a well-bonded and dense protective coating by depositing powder at ultra-high speed and various temperature regimes (Ref 1, 2). By using detonation spraying technology, high-temperature metal particles or vapors can be sprayed directly onto the surface of the substrate material at extremely high speeds, and the metal particles or vapors cool rapidly on the substrate surface to form a coating with excellent mechanical properties (Ref 3).

The manufacture cost and gas capacity of spray guns vary greatly with different designs. The flow rate, temperature and pressure at the spray gun outlet after gas detonation directly affect the performance of detonation spraying since they determine the melt state of the introduced powder particles. The actual process involves the interaction of many complex physical and chemical processes such as deflagration-to-detonation transition, two-phase flow (Ref 4), solid-phase change, effects of thermal boundary conditions and vitiation (Ref 5). The complete schematic of the detonation spray coating process is shown in Fig. 1. Gas is introduced into the gun on the left side and ignited by a spark plug, followed by the generation of a

Published online: 06 June 2024

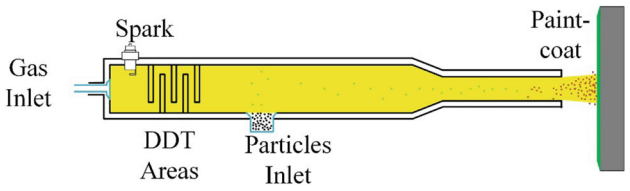

Fig. 1 Complete schematic of the detonation spray coating process

combustion flame. This flame undergoes the deflagration-to-detonation transition (DDT) process as it passes through the spiral channel. Eventually, the detonation flame melts the introduced particles and expels them onto the substrate. Fikus et al. (Ref 2) estimated the kinetic properties and thermal history of Fe40Al intermetallic compound particles using propane detonation. They noted that only particles with diameters smaller than 80 μm melted under the conditions studied. The particles used in particle image velocimetry (PIV) techniques are typically in the range of a few micrometers to tens of micrometers in diameter, which is smaller than the characteristic scale of the flow field. In this technique, the particles usually do not significantly affect the velocity field of the fluid itself. In the same principle as the PIV technique, the particles used in the experiments were 15-45 μm in diameter, which is small enough to be detected by optical imaging, which has a negligible effect on the gas dynamics, and therefore the simulation model was simplified by focusing on the gas dynamics in the simulation, and not set up with a particle pass-through. The optimum parameters can be obtained by studying the velocity and pressure at the exhaust of the nozzle.

Currently, researchers have conducted numerous studies (Ref 6) on the detonation initiation conditions (Ref 7) and flame acceleration (Ref 8) of common combustible gases in a constant diameter structure of a spray gun through theoretical (Ref 9), experimental (Ref 10), and numerical simulation methods (Ref 11-13). Ramadan et al. (Ref 14) developed a two-dimensional axisymmetric transient flow model for multi-component, variable gas properties to analyze the pulse detonation thermal spraying process. They suggested that in order to achieve high velocity, particles should be loaded at a distance from the ignition location, away from the vicinity of the explosion initiation. Gavrilenko et al. (Ref 15, 16) presented a model of the process in the cylinder of a powder coating explosion device, which takes into account the changes in the composition of the working gas in the cylinder, and they pointed out that the size of the cylinder, the volume of the mixer, the degree of cylinder filling and the position of the powder spraying have a significant effect on the parameters of the particles, which is a great instructive useful for the establishment of the model. Batraev et al. (Ref 17) gave the results of numerical simulation and experimental realization of the effect of chemical reaction airflow on powder particles in the process of combustion chamber mimicry (diameter enlargement and capacity preservation) in the cartridge of the explosion spraying device, which showed that this mimicry allows a considerable reduction in the body tube dimensions without affecting the technological performance of the detonation unit, and also pointed out that, in the studied range, the particle velocity at the exit of the barrel is determined only by the diameter of the particles, practically independently of the depth of the loading. The results of these researches are insightful and provide a foundation for the selection of particle diameters. Ulianitsky et al. (Ref 18) have analyzed the parameters of gas detonation and calculated the particle flight velocity and temperature. They pointed out that detonation spraying depends to a large extent on the accuracy of operational parameters such as the composition of the explosive mixture, the charge, the position of the powder spray, as well as on the strict control of the process parameters, and also provided the velocities that can be achieved by the detonation products, which, for hydrocarbon fuel mixtures with stoichiometric ratios, have a mass velocity of close to 1100 m/s, which is the upper limit of the particle velocities for the detonation of these mixtures. This provided the rationale for our study.

Kailasanath et al. (Ref 19) conducted numerical simulations on an ideal pulse detonation engine with one end closed and the other end open. The simulation results can be used to elucidate the detailed characteristics of the flow field and estimate the pulse of various combustible mixtures. Liu et al. (Ref 20) indicated that the presence of the first obstacle in the pipeline can reduce the hindrance of the wall boundary layer on the flame, thereby accelerating the flame propagation speed. These simulation settings provide significant guidance for the establishment of the model in this study.

Detonation waves can release tremendous energy within a short period of time, with propagation speeds reaching magnitudes of several km/s, such as in pulse detonation engines (PDEs) and rotating detonation engines (RDEs). Building upon gas detonation technology, detonation spraying has been successfully applied in engineering practice. The physical model established in this work operates similarly to a pulse detonation engine, utilizing gas detonation to achieve thermal spraying. The high temperature generated can heat the powder particles injected into the barrel, accelerating them toward the substrate. Therefore, studies on the detonation combustion are very instructive for thermal spraying.

Researchers have conducted numerous studies not only in numerical simulation, but also in experimental investigations of detonation wave propagation. J. Li et al. (Ref 21)

studied the influence of pipe diameter on the initiation distance of deflagration-to-detonation transition (DDT) through experiments. They found that the effect of pipe diameter on DDT initiation distance depends on the type and composition of the mixture, but the impact on temperature and gas velocity at the spray gun outlet has not been studied. Liu et al. (Ref 22) measured the detonation cell size of propane/oxygen/nitrogen under different initial conditions and found that increasing the initial pressure increases the concentration of fuel and oxidizer, ultimately accelerating the detonation speed. Wu et al. (Ref 23) investigated the effects of argon dilution and expansion ratio on detonation wave propagation characteristics through experiments. The results showed that within the detonation limits, the detonation speed gradually decreases with increasing initial pressure, but decreases rapidly as the initial pressure approaches the limit. Ciccarelli and Cross (Ref 24) conducted detonation experiments with hydrogen/air in a 10-cm inner diameter tube and found that the average detonation propagation velocity at the tube end is much lower than the theoretical Chapman-Jouguet (CJ) value. Xu et al. (Ref 25), through experiments conducted with a custom-designed detonation apparatus, unveiled the effects of ignition strength and pressure on the knock intensity of internal combustion engines and the formation of superknock. These findings provide valuable insights into the temperature and pressure settings within the ignition zone of this work. These experimental results provide significant validation for the conclusions drawn in this work.

Previous studies have extensively investigated detonation flame propagation and DDT processes, as well as investigations into combustion chamber structures (Ref 26) and nozzle outlet designs (Ref 27). But further research is needed to understand the impact of variable diameter structures in spray guns on gas detonation. In the design of spray gun structures, a larger diameter at the front end of the gun can meet the particle intake requirements, while a smaller diameter at the rear can enhance the accelerating effect of the gas. Additionally, when gas molecules and detonation waves encounter obstacles, reflected waves are formed, and the impact of different slope lengths (gradients) of the reflected waves on detonation varies. Furthermore, due to different blockage ratios, the formation of precursor shock waves and the magnitude of energy loss differ, resulting in variations in parameters such as gas detonation velocity at the spray gun outlet. Therefore, based on a detonation spraying gun with an overall diameter of 26 mm and a constant 20 mm diameter, an inwardly tapered slope structure is introduced at the middle position of the 26 mm diameter gun to reduce the diameter to 20 mm. Numerical simulation methods are conducted to investigate the effects of different slope lengths (5, 15, 25, 35, 45 mm) when the spray gun diameter changes from 26 mm to 20 mm. This includes studying the propagation of detonation flame velocity, the variation process at the variable diameter section, and the influence on gas flow velocity, temperature, and pressure at the spray gun outlet. The aim of this work is to determine, explore the structure effects of spray gun on overall performance and provide guidance for practical detonation spraying.

Numerical Methods and Computation Models

Conservation Equations

The detonation process of gases is described using the Navier–Stokes equations for compressible gas reactions. The conservation equations for mass, momentum, energy and components of the mixture are expressed as follows:

$$\frac{\partial \rho}{\partial t} + \nabla \cdot (\rho u) = 0 \quad \text{(Eq 1)}$$

$$\frac{\partial \rho u}{\partial t} + \nabla \cdot (\rho u u) = -\nabla p + \nabla \cdot \tau \quad \text{(Eq 2)}$$

$$\frac{\partial \rho H}{\partial t} + \nabla((\rho H + p)u) = \nabla \cdot (\tau \cdot u) - \nabla \cdot q + \dot{\omega}_T \quad \text{(Eq 3)}$$

$$\frac{\partial \rho Y_i}{\partial t} + \nabla \cdot (\rho Y_i u) + \nabla \cdot J_i = \dot{\omega}_i \quad \text{(Eq 4)}$$

$$H = h + 0.5u^2 - \frac{p}{\rho} \quad \text{(Eq 5)}$$

where ρ is the density of the mixture; u is the velocity; p is the static pressure; τ is the viscous stress satisfying the Stokes hypothesis; H is the total energy of the mixture and h is the apparent enthalpy; $\dot{\omega}_T$ is the heat of combustion; Y_i is the mass fraction of the component (i = 1,...,n); ω_i is the reaction rate of the component; J_i and q are the mass diffusion flux and heat flux of component I, respectively. (Ref 28, 29).

Based on the turbulent kinetic energy and turbulent dissipation rate, and taking into account the effect of shear stress on the wall of the turbulent gas in the confined space, the transport equation with the limiting vortex viscosity of gas transport is chosen in this paper, which is expressed as follows:

$$\frac{\partial}{\partial t}(\rho k) + \frac{\partial}{\partial x_i}(\rho k u_i) = \frac{\partial}{\partial x_i}\left[\left(\mu + \frac{\mu_i}{\sigma_k}\right)\frac{\partial}{\partial x_j}\right] + G_k - Y_k \quad \text{(Eq 6)}$$

$$\frac{\partial}{\partial t}(\rho \omega) + \frac{\partial}{\partial x_i}(\rho \omega u_i) = \frac{\partial}{\partial x_i}\left[\left(\mu + \frac{\mu_i}{\sigma_\omega}\right)\frac{\partial \omega}{\partial x_j}\right] + G_\omega - Y_\omega + D_\omega \quad \text{(Eq 7)}$$

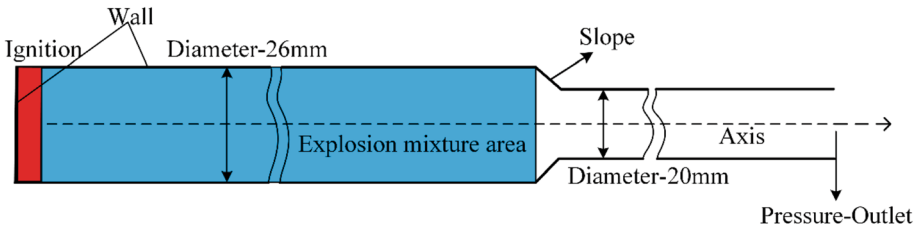

Fig. 2 Two-dimensional physical model of the spray gun

$$\xi^* = C_\xi \left(\frac{v}{K^2}\right)^{\frac{1}{4}} \quad \text{(Eq 8)}$$

$$R_i = \frac{\rho(\xi^*)^2}{\left(1-(\xi^*)^3\right)}\left(Y_i^* - Y_i\right) \quad \text{(Eq 9)}$$

where G_k is the turbulence fluctuation generated by the velocity gradient; G_ω is the generation term of the turbulence fluctuation frequency ω; Y_k and Y_ω are the consumption term, respectively; D_ω is the cross-diffusion term, σ_k and σ_ω are the turbulence Prandtl numbers of k and ω, respectively; ξ^* is the length coefficient of the small-scale vortices; C_ξ is the volume ratio constant; C_ξ = 2.1377, v is the kinematic viscosity and Y_i^* is the mass fraction of τ^* component i after the reaction time.

Physical Model

The geometrical model of the spray gun designed in this paper is shown in Fig. 2 and 3. A two-dimensional axisymmetric model (Ref 20, 30) was used to simulate the effect of different gun configurations on gas detonation. The right outlet boundary condition of the gun model is the pressure outlet, and the rest of the boundary conditions are adiabatic no-slip walls. The model consists of two sections with different diameters, a 26-mm-diameter section with a length of 550 mm, and a 20-mm-diameter section connected to the first section using different reducer lengths (5, 15, 25, 35 and 45 mm). The total length of the nozzle is kept at a constant 850 mm length. Based on the engineering practice, propane was chosen as the fuel for the simulations and experiments (Ref 33-34). Prior to the start of the simulation, 21% oxygen and 79% nitrogen were used as the ambient conditions in the full calculation domain of the bursting gun, and the volume π*(0.013 m)^2 *0.54 m $\approx$ 287 ml before the reducer was filled with pre-mixed propane and oxygen to ensure that the same amount of gas was used as fuel for different reducer gun configurations. The mixture equivalence ratio φ was 1.0.

The initial pressure in the blast gun is atmospheric pressure, and the initial temperature is 303 K. In order to study the parameter changes at the exit of the gun, the model ignores the initial stage of deflagration to detonation in the spiral tube, high-temperature and high-pressure ignition instead of the spiral tube channel to generate a

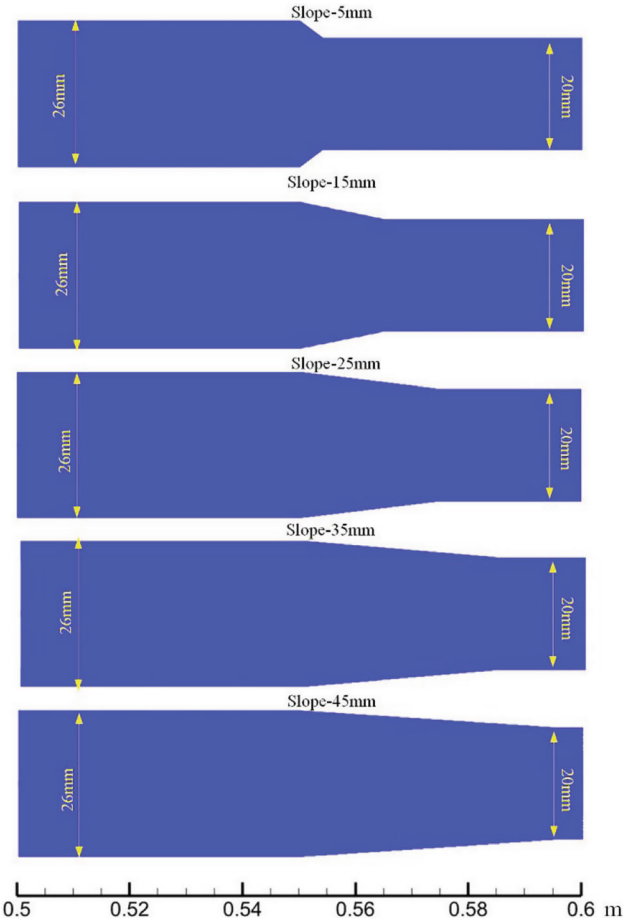

Fig. 3 Comparison of different spray gun structures

detonation wave to achieve the same detonation effect. In the current study, the detonation is triggered by setting the ignition zone volume π*(13 mm)^2*10 mm $\approx$ 5.31 ml at the left end of the gun. The parameters of the ignition zone were set by setting the temperature at 2500 K and the pressure at 8 MPa according to previous studies and estimation of the energy required for direct detonation (Ref 34-36), and this ignition condition was used for all simulations. The time between the ignition of the gas mixture in the blast gun and the formation of the blast wave is extremely short so that the heat exchange process between the flame surface and the wall surface of the blast gun during the detonation process can be neglected (Ref 37).

Table 1 Model settings in simulation

Turbulence model	SST (Shear stress transmission) $k-\omega$
Combustion model	Eddy dissipation concept (EDC)
Algorithm	PISO
Wall conditions	Adiabatic non-slip

Hence, the isothermal walls with a temperature of 303 K were adopted in the model.

A reduced 26-component 34-step mixed-fuel chemical reaction mechanism obtained by simplifying a 357-step detailed chemical reaction mechanism (Ref 38) was used for propane combustion. This mechanism can accurately predict the chemical reaction characteristics in the fuel bombardment process (Ref 20). The chemical reaction model employs the Eddy dissipation concept (EDC) model to address multi-step chemical reaction mechanisms. Conservation equations were discretized by the finite volume method in the Ansys Fluent computational dynamics software. Momentum equations are closed by the SST k-ω turbulence model and solved by the pressure-based PISO algorithm. The time step of the calculation is chosen to be 1e−6 s (Ref 2, 20).

The model settings are shown in Table 1.

To achieve a more precise calculation of the gas detonation effects, the grid adaptive refinement feature is activated to refine the calculation of flame front propagation, with the maximum refinement level set to 2.

The calculation zone is divided into different numbers of cells uniformly. The grid size Δx = 0.2, 0.5, 0.8 mm is chosen to derive the optimum grid scale for the computational domain. The time difference of the blast wave under different grids is obtained by monitoring the temperature at the gun outlet over time, as shown in Fig. 4. The generation of the blast wave at Δx = 0.8 mm lags significantly behind that of the blast wave under the grid sizes of 0.2 mm and 0.5 mm, and there is no significant difference between Δx = 0.2 mm and Δx = 0.5 mm. Therefore, a grid size of Δx = 0.5 mm was chosen to balance the computational cost and accuracy.

Experimental Verification

To validate the constructed model, propane gas detonation experiments were conducted in a spray gun with a slope length of 5 mm. WC-12Co particles (particle size 15–45 μm) (Ref 2, 36) were introduced into the spray gun at a distance of 350 mm from the gun outlet, melted by the high temperature generated by the gas detonation, and expelled from the gun during the gas detonation process. High-speed

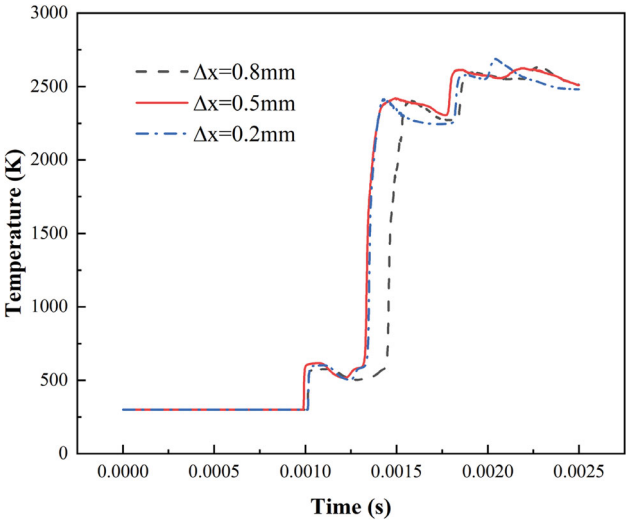

Fig. 4 Temperature changes at the spray gun outlet for different grid sizes

camera X213M produced by Fuhuang Junda High Tech Information Technology Co., Ltd was used to capture the particles at the exit position of the spray gun, with an exposure time of 1 μs, and lens with a focal length of 105 mm, with a frame rate of 37,037 frames. Utilizing ImageJ software for the analysis of captured particle images imports a calibration scale and applies color-coding and numbering to the lines, as shown in Fig. 5. The image was first pre-processed to greyscale, then the length of thin lines in the image was measured to adjust the valve threshold, and finally the overlapping thin lines were excluded using the area selection method. The length of the trajectory lines in the captured photographs was measured [18], and the velocity analysis was performed using the velocity formula V = L/t (where L is the length and t is the time), in order to obtain the velocities at different stages of the pulsed flame. The schematic diagram of the velocity measurement principle is shown in Fig. 6.

Velocities were measured for particles sprayed from propane gas detonations carried out in a gun structure with a diameter of 26 mm. The measured velocity of particles at the spray gun outlet is compared with the simulated gas velocity [Refs 2, 36], as shown in Fig. 7. The trend of the velocities obtained from the experiment and the simulation was the same for a certain period of time, beginning with a rapid increase in velocity and then changing to a steady propagation. The average particle velocity calculated from the experimental measurements is 1119.7 m/s, and the average gas velocity in the simulation is 1106.97 m/s, which is a very high degree of agreement of the average velocities. The average velocities all exceed 1000 m/s, and the relative error of the simulation is 6.39%. Due to the particle melting, a portion of energy is consumed during

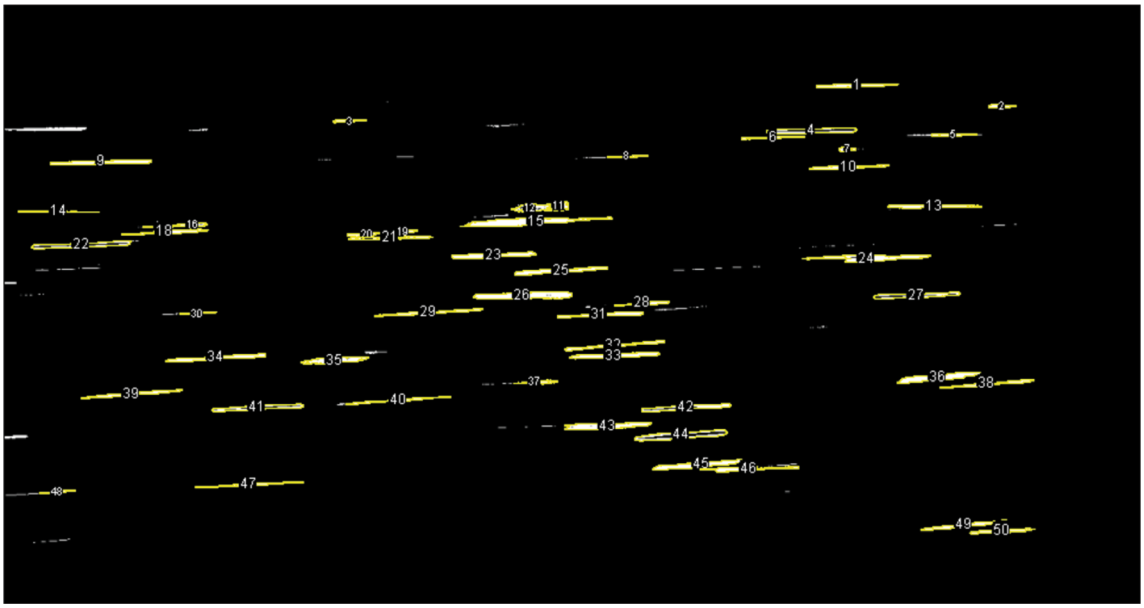

Fig. 5 Capture particle images using a high-speed camera and perform post-processing

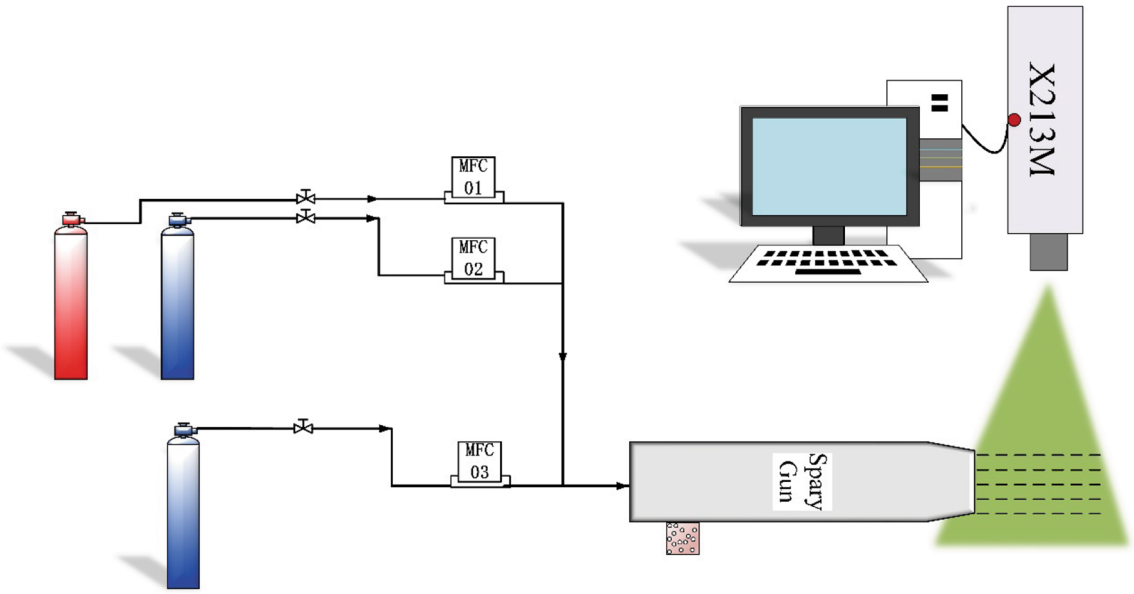

Fig. 6 Schematic diagram of the measuring principle

the explosion process (Ref 39). Therefore, without considering this process, the simulation results show a slight discrepancy compared to the experimental data calculated using high-speed camera photographs. The reason for the higher speed of the experimental measurements than of the simulation calculation may be that the simulation setup (heat conduction, ideal gases, etc.) produced small errors. However, the error does not exceed 7%, which is within an acceptable range.

Results and Discussion

Multi-physics Fields Analysis

Analyzing the velocity, temperature, and pressure generated by gas detonation is crucial for understanding the behavior and performance of detonations. These parameters are significant because they provide valuable insights

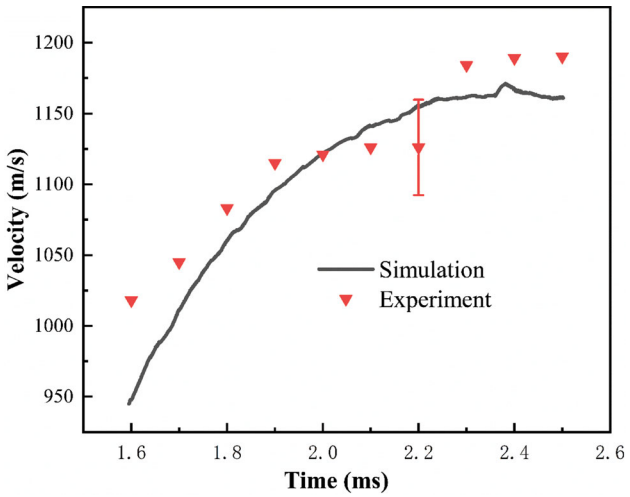

Fig. 7 Comparison of experimental and simulation velocity

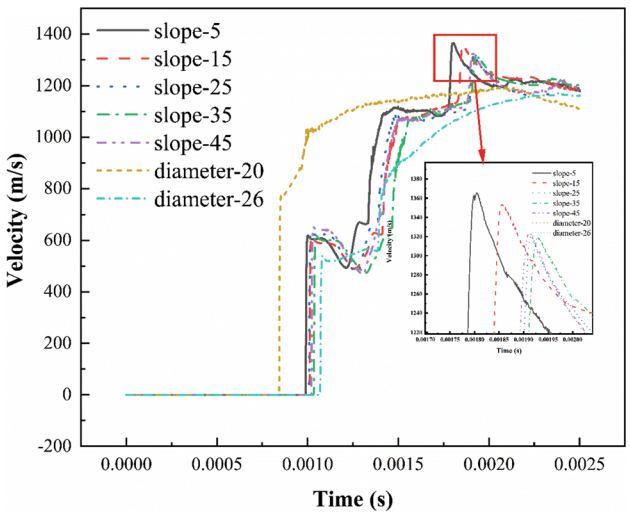

Fig. 8 Velocity variation at the outlet of different spray gun designs

into the efficiency, power, and safety of the detonation process. To provide a clear illustration of the differences in detonation between constant diameter and various variable diameter gun structures, simulations are conducted using a constant diameter gun model of 26 mm and 20 mm, as well as five different gun models with varying slope lengths (5, 15, 25, 35, and 45 mm).

In depositing high-quality coatings, new technologies promoting a high velocity of material deposition are needed. Higher velocity of sprayed particles usually leads to a more compact surface on the sprayed structure, resulting in improved performance. Figure 8 depicts the temporal variation of gas velocity at the gun exit under different throat slope lengths. Notably, the gun exit of a 20-mm-diameter pipeline achieves its maximum velocity in the shortest time. This phenomenon is attributed to the influence of the boundary layer (Ref 4). The interaction between the reflected shock waves and the incoming detonation wave creates a recirculation zone where the gas flow is significantly disturbed. In this region, gases are effectively trapped and recirculated, as shown in Fig. 9 at a detonation time of 0.7 ms. Consequently, in cases of smaller gun diameters, hot spots are more prone to form within the boundary layer, intensifying chemical reactions. This leads to a faster increase in gas velocity and a shorter time to reach supersonic detonation.

Conversely, for a gun diameter of 26 mm, the time taken to achieve the highest velocity at the gun exit is longer. Moreover, the maximum attainable gas velocity is noticeably lower than that of a 20-mm gun diameter and the gun with a diameter change. Three distinct peaks in the gas velocity profile at the gun exit indicate the presence of three acceleration cycles within the gun (attributed to three turning points). Following three acceleration cycles, the pipe with a length of 5 mm at the point of diameter variation reaches its maximum gas velocity at the gun exit in 1.80 ms, with a peak velocity of 1365.21 m/s. Subsequently, as the length of the slope at the gun's transition section increases, it sequentially attains its highest gas velocities. The diameter change gun with a 5-mm throat slope exhibits the highest variation, and its ability to achieve higher flow velocities due to the compressibility effects of gases is more obvious. The faster the velocity of the spray gas flow generated by the gas detonation, the higher the velocity of the sprayed particles carried can be achieved, while the higher particle velocity leads to higher coating density and adhesive strength, when other factors are certain (Ref 40, 41).

A higher temperature means greater internal energy within the gas, contributing to the overall energy output of the detonation process. This is particularly important in applications where high energy release is required. Figure 10 presents the temporal temperature profiles at the gun outlet for various reducer slope lengths. Notably, the 20-mm diameter gun exhibits the most rapid temperature increase, while a consistent temperature trend is observed across all gun configurations at the outlet. On the other hand, the 26-mm diameter gun displays the slowest rise in outlet temperature and attains the lowest maximum temperature compared to other gun setups. The gun outlet with a 5-mm reducer slope length demonstrates the fastest attainment of the highest temperature after three cycles of temperature increase. However, the 25-mm reducer slope length obtains the highest temperature at the gun outlet, reaching a value of 2703.13 K.

The change in gas density directly affects the rate and efficiency of combustion. The combustion process can be better understood by investigating the changes in gas density. Figure 11 shows the density as a function of time

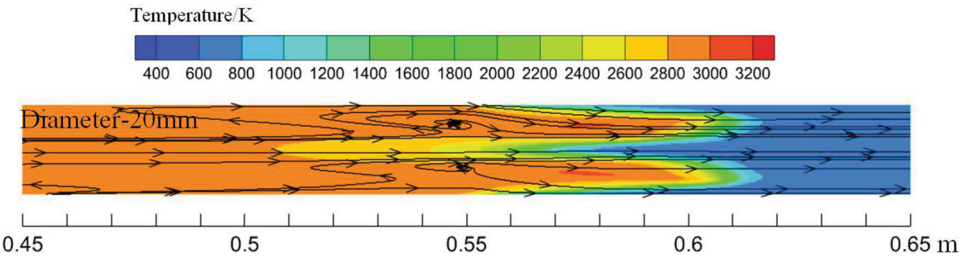

Fig. 9 Temperature and streamlines at the hotspot at 0.7 ms

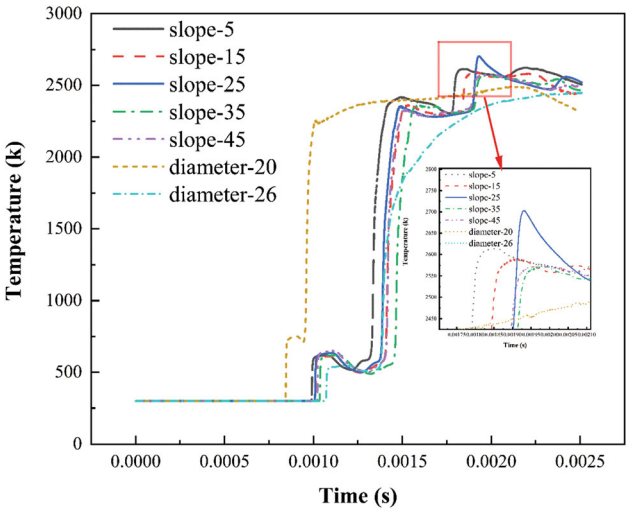

Fig. 10 Temperature changes at the outlet of spray guns with different structures

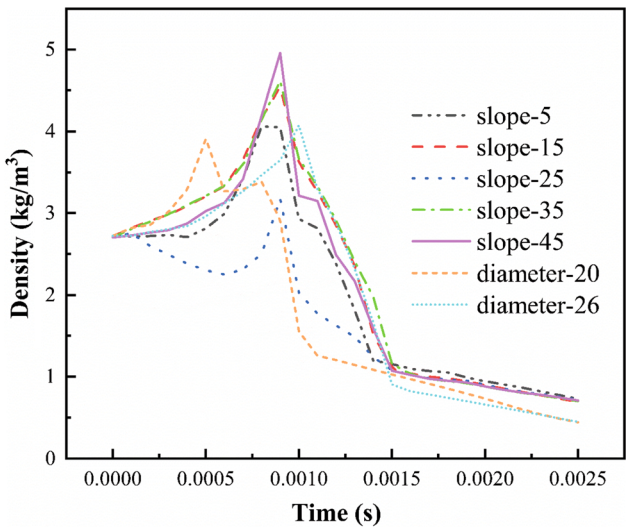

Fig. 11 Density changes at the axis of spray guns with different structures

on the axis of different structures of spray guns. The mixing of fuel and oxidant was more concentrated, and the combustion reaction was more rapid in the 20-mm diameter gun, with the shortest time for density to reach the maximum value of 0.5 ms; the mixing and combustion

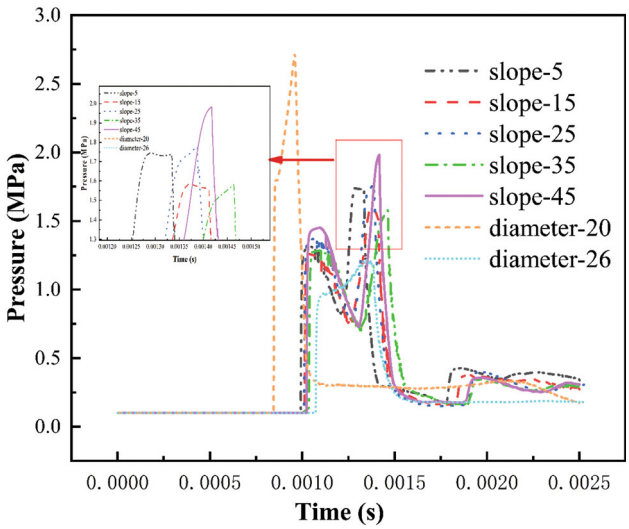

Fig. 12 Variations of pressure with time at the outlet of spray guns with different structures

process was relatively slower in the 26-mm diameter gun, with the longest time for the density to reach the maximum value of 1.0 ms. In the gun with the change of the diameter, the densities of all the cases reach the maximum value at 0.9 ms. Maximum value of the slope length of 45-mm structure in the process of detonation to provide a more adequate mixing and larger combustion area reached the largest gas density of 4.96 kg/m^3; slope length of 25-mm structure combustion efficiency is relatively low, and reached the smallest gas density of 3.18 kg/m3. The gun density reached the maximum value, with the detonation, and the combustion product gradually occupies the more space, and the gas density starts to decrease in all cases.

Studying and controlling the outlet pressure of a gas detonation system is imperative for safety, operational efficiency, and performance optimization. It prevents accidents, and ensures predictable and controlled detonation processes. Figure 12 presents the pressure–time curves at the outlet of the gun for different lengths of reducer slope. It is evident that the outlet pressure of the gun varies depending on the configuration. Specifically, the gun with a tube diameter of 20 mm consistently achieves a significantly higher outlet pressure compared to the other configurations. On the other hand, the gun with a tube diameter

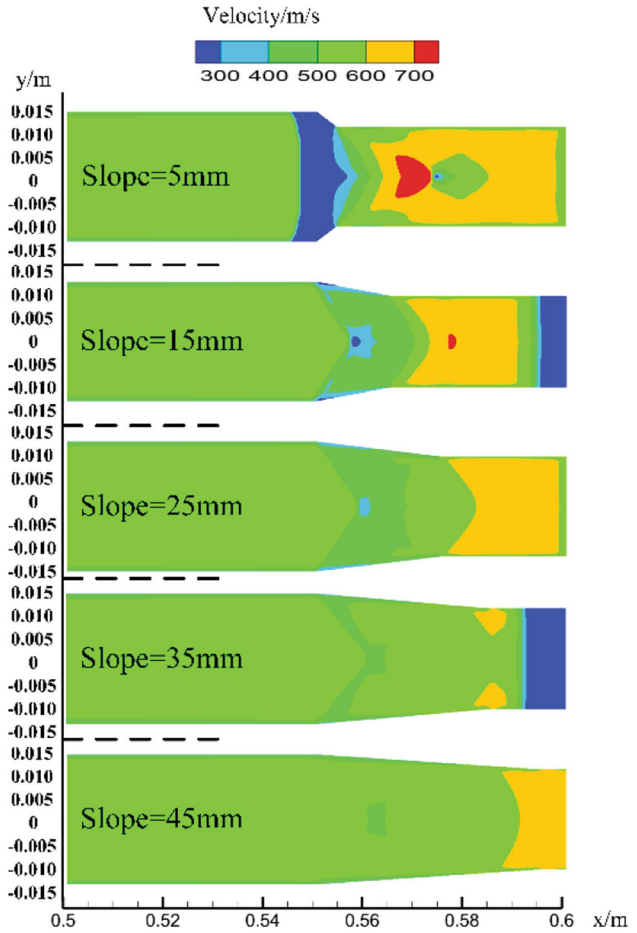

Fig. 13 Comparison of velocity under different nozzle slopes with variable diameter at 0.7 ms

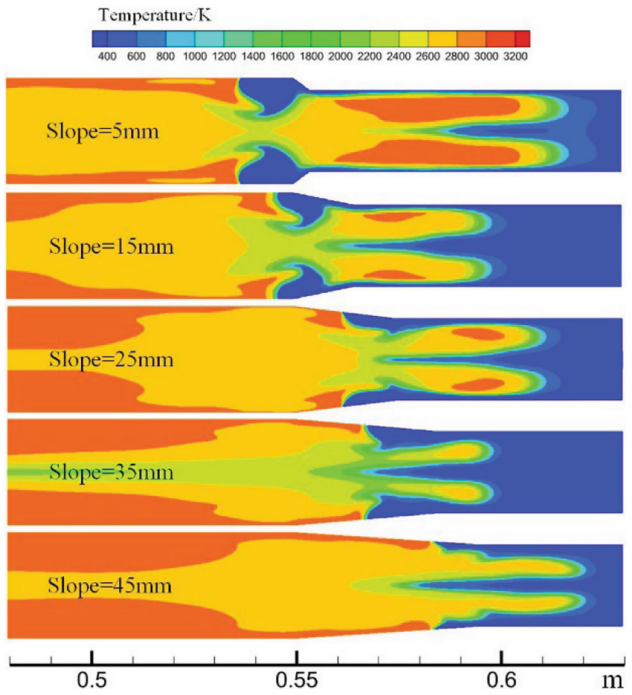

Fig. 14 Comparison of temperature under different spray guns with variable diameter slopes at 1.0 ms

of 26 mm demonstrates the lowest outlet pressure. Notably, among the spray guns with variable diameters, the maximum outlet pressure of 1.98 MPa is observed in the spray gun with a variable diameter of 45 mm.

Effects of Different Slope Lengths

When the gun diameter undergoes alterations, it exerts an influence on the detonation characteristics generated at the gun exit. Furthermore, changes in the slope length (or gradient) at the gun throat have distinct effects on the propagation of the detonation wave. As the detonation wave reaches the sloped obstacle at the gun throat, it engenders a reflected wave, thereby impacting various propagation characteristics of the detonation, including gas flow velocity, temperature, and pressure.

Figure 13 illustrates the velocity contours of the gas at 0.7 ms for different lengths of the reducer slope. The expansion wave produced by the deflagration collides with the barrier, which can result in a more intense reflected wave. This reflected wave impedes the flame propagation on the upper and lower sides, redirecting the flame toward the center and causing deformation of the flame front. Consequently, the curvature of the flame front undergoes a rapid increase. Moreover, the chemical reaction rate and turbulent kinetic energy intensity of the flame front are enhanced, leading to an accelerated flame propagation speed (Ref 22). The flame propagation speed continues to increase as the flame front traverses the obstacle.

A comparison of the contour diagrams reveals that the reflection of the expansion wave on the windward side of the obstacle is most pronounced when the reducer slope length is 5 mm, resulting in the greatest increase in flame propagation speed and consequently the highest gas flow rate. The increase in gas velocity decreases as the reducer slope length becomes larger. This finding aligns with the variations observed in the gas flow velocity at the gun outlet, whereby the greatest gas flow velocity can be achieved with a reducer slope length of 5 mm.

Flame front contours at the 1.0-millisecond time were shown to investigate the impact of nozzle diameter variation on flame propagation. This time frame is chosen as the flame front propagation velocity typically lags behind the expansion wave propagation by approximately 0.3 milliseconds. Figure 14 presents the temperature contour of the variable diameter structures of different guns at 1.0 ms. Analyzing the acceleration effect exerted on each gun flame through the reducer in Fig. 14, and it becomes apparent that a gun structure with a reducer slope length of

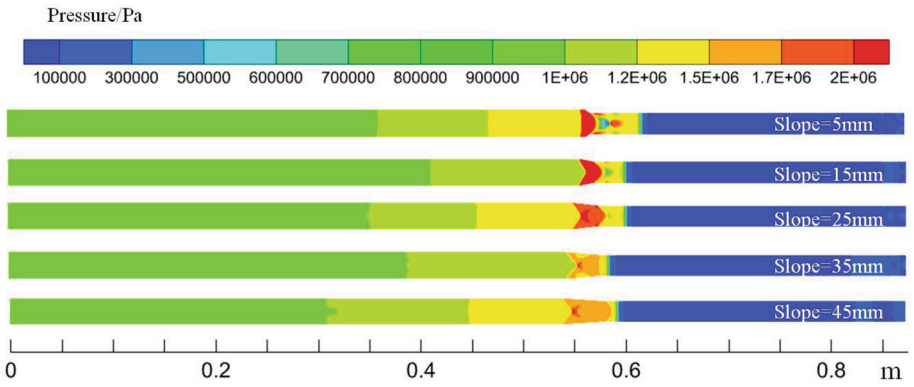

(a) Total gun pressure contours.

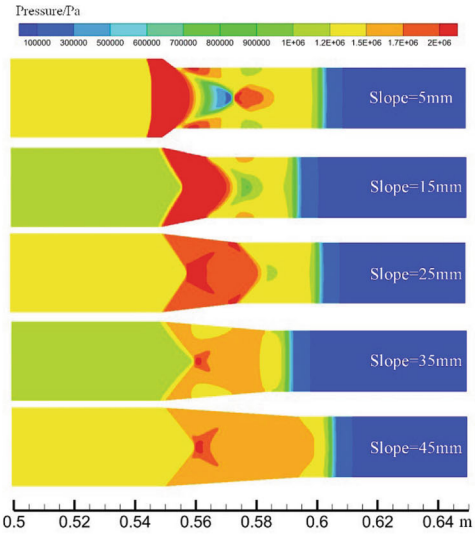

(b) Pressure contours at the different slope lengths.

Fig. 15 Comparison of pressure under different spray guns with variable diameter slopes at 0.7 ms

5 mm exhibits a more significant influence on flame acceleration.

In comparison with the flame in the middle of the gun pipe, the flame near the pipe wall propagates at a faster rate, leading to the formation of a funnel-shaped flame in the center of the pipe. At the gun reducer ramp, reflux zones are formed on both the upper and lower walls. The interaction between the expansion wave generated by the flame and the wall of the gun pipe results in the formation of a reflected wave. Under the influence of this reflected wave, the chemical reaction rate gradually increases and, consequently, the amount of heat released also increases. As the length of the reducer slope increases, the reflux zone formed by the reflected wave progressively diminishes, leading to a decrease in the flame acceleration effect. Collisions in gas detonation not only result in energy loss, but also lead to lower temperatures in the region of action of the reflected shock wave, thereby reducing the overall temperature. Additionally, a comprehensive comparison between the heating effect of the reflected shock wave and the energy loss caused by collisions is conducted, and the results indicate that gas detonation can reach higher temperatures under a spray gun with a slope length of 25 mm.

Figure 15(a) illustrates the comprehensive pressure distribution in the gun with various lengths of reducer slopes at 0.7 ms. In Fig. 15(b), the pressure distribution is displayed for different gun reducers. In gas detonation, the detonation wave collides with obstacles on the windward side as it passes through the nozzle throat, generating a reflected shock wave. The detonation wave and the reflected shock wave interact with each other in a finite space. As a result, local pressure rapidly increases and accelerates the propagation of shock waves. At the same time, the reflected shock wave suppresses the forward propagation of the detonation wave. Although smaller slope lengths exhibit more pronounced shock waves within

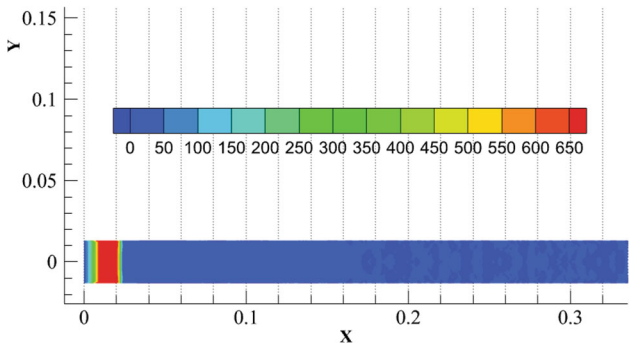

Fig. 16 Gas velocity contour in the gun at 0.01 ms

the spray gun, the shock waves do not fully convert into forward-propagating expansion waves. Most of the shock waves are consumed on the wall surface of the nozzle throat. In the spray gun structure after the nozzle throat, the structure with a slope length of 45 mm exhibits the most significant promotion of gas pressure increase, leading to a significant overall pressure elevation within the spray gun.

The Flame Propagation Process

In propane gas detonation stage shown in Fig. 16, the propagation distance of the detonation wave at 0.01 ms is about 0.024 m, and the calculated propagation velocity of the detonation wave is 2400 m/s. The theoretical detonation velocity of the propane mixture is 2358 m/sec (Refs 42, 43), and the simulations at the beginning of the detonation exceed the theoretical detonation velocity of the mixture. Then, focus on the study of the process of change of the detonation wave through the gun reducer.

To provide a clear depiction of the changes in the bursting gas flame before and after passing through the gun reducer, a gun structure with a reducer slope length of 5 mm was chosen to illustrate the gas flow rate, temperature, and pressure changes occurring within the first acceleration cycle from 0.6 to 1.2 ms in Fig. 17(a)–(c). The contour diagrams show the variations in gas flow rate, temperature, and pressure during the initial acceleration phase.

During detonation, the flame front moves at a velocity faster than the expansion wave. At $t = 0.8$ ms, the expansion wave encounters an obstacle at the changing diameter, resulting in the formation of a reflected wave. This collision hinders the flame from spreading toward the inclined wall of the nozzle, causing deformation in the flame front. Upon passing through the nozzle, the depth of the funnel shape decreases, accompanied by a reduction in nozzle diameter, diminishing the impact of the upper and lower wall surfaces on flame propagation.

After the flame front passes through the area of change in gun diameter, the flame front experiences a rapid increase in velocity, leading to an increase in pressure wave. The intensity of the pressure wave surpasses 1 MPa, thereby forming a shock wave. The leading shock wave enhances the thermodynamic state of the unburned gas mixture existing between the flame and the shock wave, consequently elevating the reaction rate and accelerating flame propagation. Simultaneously, as the flame traverses the transition point of the spray gun, the temperature and pressure of the flame front decrease due to energy loss caused by the slope of the spray gun.

These findings align with the alterations observed in gas flow rate, temperature, and pressure at the spray gun outlet, with the maximum achievable values serving as the basis for adjusting various spray gun structures.

Conclusions

This work presents a detailed study of the propagation characteristics of propane/oxygen/nitrogen mixed gas detonation flames and the parameter changes at the nozzle outlet under different spray gun structures using two-dimensional CFD simulation. At a constant detonation gun tube diameter, a smaller nozzle diameter achieves higher flow rates, temperatures and pressures at the gun outlet because it promotes the formation of hot spots in the boundary layer. The exit velocity, temperature, and pressure of the 20-mm diameter gun increased by 1.36, 1.36, and 1.25 times, respectively, compared to the 26 mm. The use of variable diameter structures has a significant effect on the detonation process. Different slope lengths in the gun yield varying acceleration effects on the detonation wave and flame front, leading to significant disparities in the velocity, temperature, and pressure generated by the gas detonation within the gun. The maximum gas velocity at the gun outlet is the highest when the gun reducer slope length is 5 mm, and the detonation wave exhibits the most effective acceleration in this configuration. The peak temperature at the gun outlet is maximum when the gun reducer slope length is 25 mm, and the local hot spot generates the most efficient temperature increase in this configuration. The gun outlet pressure is maximum when the length of the reducer slope is 45 mm, and there is a minimal loss of energy in this configuration. For temperature and velocity requirements of spraying different substrates and particles, the selection of suitable gun configurations can be based on the results obtained from this simulation.

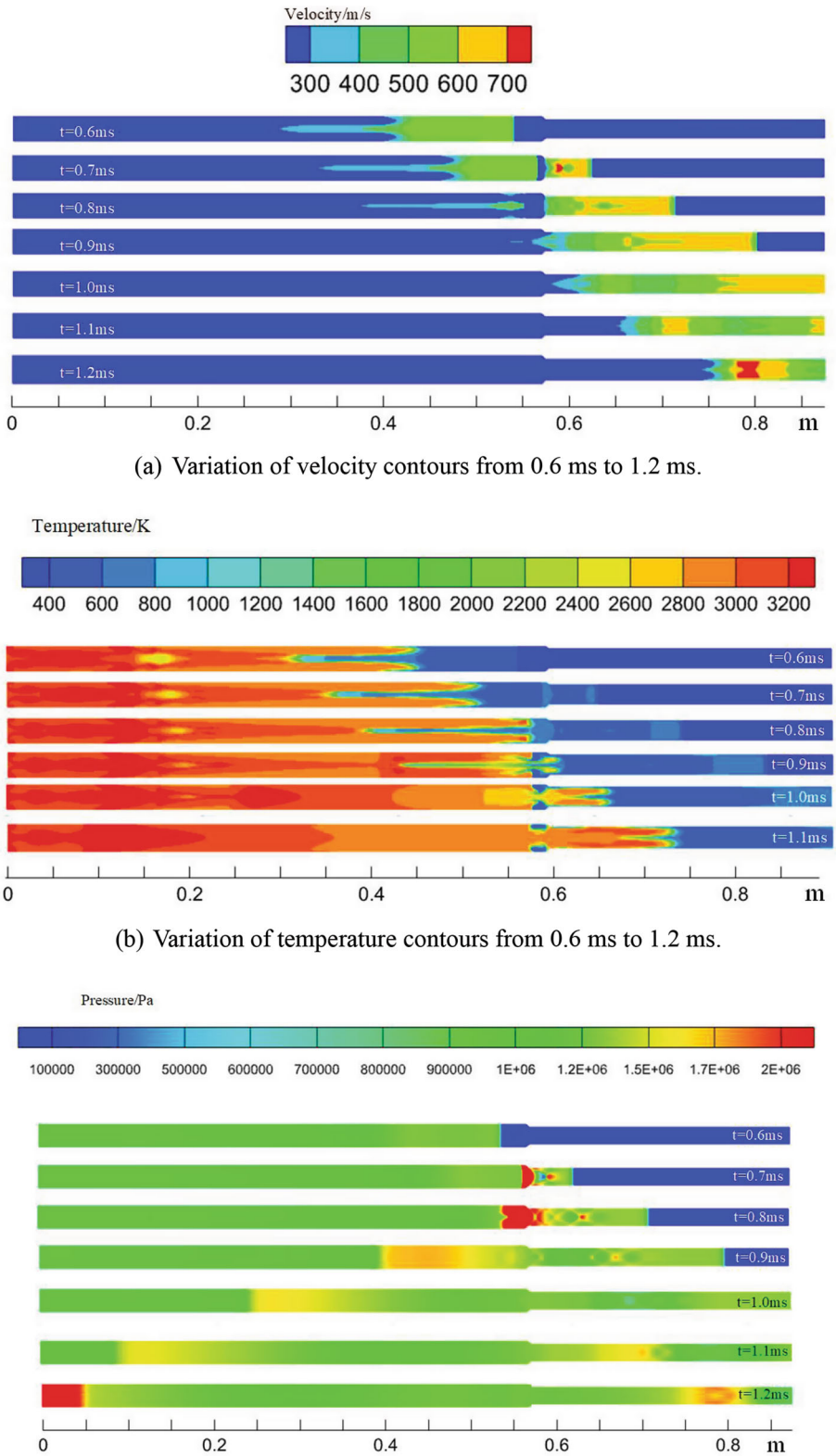

Fig. 17 Contours of velocity, temperature, and pressure changes with a variable slope length of 5 mm

Acknowledgment This work is supported by the National Natural Science Foundation of China (52325604), the National Science and Technology Major Project (J2019-III-0005-0048), MOST (2021YFA0716200/2022YFB4003900), CAS Project for Young Scientists in Basic Research (YSBR-028) and the Innovation Academy for Light-duty Gas Turbine, Chinese Academy of Sciences, Innovation guidance youth project (CXYJJ21-QN-001).

References

1. C. Senderowski, A. Panas, B. Fikus, D. Zasada, M. Kopec, and K. Korytchenko, Effects of Heat and Momentum Gain Differentiation during Gas Detonation Spraying of FeAl Powder Particles into Water, *Materials*, 2021, **14**, p 7443.
2. B. Fikus, C. Senderowski, and A. Panas, Modeling of Dynamics and Thermal History of Fe40Al Intermetallic Powder Particles Under Gas Detonation Spraying Using Propane-Air Mixture, *J Therm Spray Tech*, 2019, **28**, p 346-358.
3. Z. Pu, K. Yang, Z. Liu, and X. Mao, Numerical Simulation of Temperature Field During Electrothermal Explosion Spray Coating, *J. Mech. Eng.*, 2005, **41**, p 142.
4. S. Yao, X. Tang, and W. Zhang, Structure of a Heterogeneous Two-Phase Rotating Detonation Wave with Ethanol-Hydrogen-Air Mixture, *Phys. Fluids*, 2023, **35**, p 031712.
5. S. Ramachandran, N. Srinivasan, Z. Wang, A. Behkish, and S. Yang, A Numerical Investigation of Deflagration Propagation and Transition to Detonation in a Microchannel with Detailed Chemistry: Effects of Thermal Boundary Conditions and Vitiation, *Phys. Fluids*, 2023, **35**, p 0155645.
6. W. Han, Y. Gao, and C.K. Law, Flame Acceleration and Deflagration-to-Detonation Transition in Micro-and Macro-Channels: An Integrated Mechanistic Study, *Combust. Flame*, 2017, **176**, p 285.
7. A. Wang, J. Bian, and H. Teng, Numerical Study on Initiation of Oblique Detonation Wave by Hot Jet, *Appl. Therm. Eng.*, 2022, **213**, p 118679.
8. S. Zhao, Y. Fan, H. Lv, and B. Jia, Effects of a Jet Turbulator Upon Flame Acceleration in a Detonation Tube, *Appl. Therm. Eng.*, 2017, **115**, p 33.
9. Y. Liu, H. Shen, D. Zhang, and Z. Jiang, Theoretical Analysis on Deflagration-to-Detonation Transition, *Chinese Phys. B.*, 2018, **27**, p 084703.
10. J. Cheng, B. Zhang, H. Liu, and F. Wang, Experimental Study on the Effects of Different Fluidic Jets on the Acceleration of Deflagration Prior its Transition to Detonation, *Aerosp. Sci. Technol.*, 2020, **106**, p 106203.
11. D. Kessler, V. Gamezo, and E. Oran, Simulations of Flame Acceleration and Deflagration-to-Detonation Transitions in Methane-Air Systems, *Combust. Flame*, 2010, **157**, p 2063.
12. F. Zhou, N. Liu, and X. Zhang, Numerical Study of Hydrogen-Oxygen Flame Acceleration and Deflagration to Detonation Transition in Combustion Light Gas Gun, *Int. J. Hydrogen Energy*, 2018, **43**, p 5405.
13. K. Iwata, Numerical Approach to Theoretical Aspects of Wedge-Induced Oblique Detonation Wave in a Hydrogen Concentration Gradient, *Phys. Fluids*, 2023, **35**, p 0156540.
14. K. Ramadan and P.B. Butler, A Two-Dimensional Axisymmetric Flow Model for the Analysis of Pulsed Detonation Thermal Spraying, *Combust. Sci. Technol.*, 2003, **175**, p 1649.
15. T. Gavrilenko, Y. Nikolaev, V. Ulianitsky, M. Kim, and J. Hong. Computational code for detonation spraying process. In *ITSC* 1998 (pp. 1475-1483). ASM International.
16. T.P. Gavrilenko and Yu.A. Nikolaev, Calculation of Detonation Gas Spraying, *Combust. Explos. Shock Waves*, 2007, **43**, p 724-731.
17. I.S. Batraev, E.S. Prokhorov, and V.Y. Ul'yanitskii, Acceleration and Heating of Powder Particle by Gas Detonation Products in Channels with Cone Transition, *Combust. Explos. Shock Waves*, 2014, **50**(3), p 1-9.
18. V. Ulianitsky, A. Shtertser, S. Zlobin, and I. Smurov, Computer-Controlled Detonation Spraying: From Process Fundamentals Toward Advanced Applications, *J. Therm. Spray Technol.*, 2011, **20**(4), p 791-801.
19. K. Kailasanath, G. Patnaik, and C. Li, The Flowfield and Performance of Pulse Detonation Engines, *P. Combust. Inst.*, 2002, **29**, p 2855.
20. S. Liu, Research on Deflagration to Detonation Transition Characteristics and Mechanism of Gas-phase Propane, Harbin Engineering University, 2021 (**in Chinese**).
21. J. Li, W.-H. Lai, and K. Chung, Tube Diameter Effect on Deflagration-to-Detonation Transition of Propane-Oxygen Mixtures, *Shock Waves*, 2006, **16**, p 109.
22. S. Liu, X. Chen, N. Zhao, H. Zheng, and X. Jia, Experimental Study on Initiation and Propagation Behavior of Propane/Oxygen/Nitrogen Detonation Wave, *Fuel*, 2021, **293**, p 120487.
23. Y. Wu, Q. Zheng, and C. Weng, An Experimental Study on the Detonation Transmission Behaviours in Acetylene-Oxygen-Argon Mixtures, *Energy*, 2018, **143**, p 554.
24. G. Ciccarelli and M. Cross, On the Propagation Mechanism of a Detonation Wave in a Round Tube with Orifice Plates, *Shock Waves*, 2016, **26**, p 587.
25. H. Xu, X. Ni, X. Su, C. Weng, and C. Yao, The Effect of Ignition Intensity and in-Cylinder Pressure on the Knock Intensity and Detonation Formation in Internal Combustion Engines, *Appl. Therm. Eng.*, 2022, **200**, p 117690.
26. R. Zou, J. Liu, and N. Wang, Effect of Recess Shape on Combustion Performance and Knocking Characteristics for a Downsized Gasoline Rotary Engine, *Appl. Therm. Eng.*, 2022, **214**, p 118758.
27. Y. Zhu, K. Wang, M. Zhao, Z. Wang, and W. Fan, Experimental Study on Wave Propagations in a Rotating Detonation Chamber with Different Outlet Configurations, *Acta Astronaut.*, 2022, **200**, p 388.
28. C. Jiang, J. Pan, J. Weng, J. Li, and E.K. Quaye, Role of Concentration Gradient in the Re-initiation of H_2/O_2 Detonation in a 90° Bifurcated Channel, *Aerosp. Sci. Technol.*, 2022, **120**, p 107281.
29. C. Jiang, J. Pan, Y. Zhu, J. Li, H. Chen, and E.K. Quaye, Influence of Concentration Gradient on Detonation Re-initiation in a Bifurcated Channel, *Fuel*, 2022, **307**, p 121895.
30. G. Goodwin, R. Houim, and E. Oran, Effect of Decreasing Blockage Ratio on DDT in Small Channels with Obstacles, *Combust. Flame*, 2016, **173**, p 16.
31. C. Movileanu, M. Mitu, V. Giurcan, D. Razus, and D. Oancea, Quenching Distances, Minimum Ignition Energies and Related Properties of Propane-Air-Diluent Mixtures, *Fuel*, 2020, **274**, p 117836.
32. Y. Ruiguang, L. Jie, and M. Biao, Effect of Methanol on Explosion Limits of Propane-Oxygen Mixture, *CIESC J.*, 2021, **72**, p 3411.
33. D. Yap, J. Karlovsky, A. Megaritis, M. Wyszynski, and H. Xu, An Investigation into Propane Homogeneous Charge Compression Ignition (HCCI) Engine Operation with Residual Gas Trapping, *Fuel*, 2005, **84**, p 2372.
34. Y. Mu, D. Zheng, Y. Wang, L. Li, and H. Zhang, Numerical Simulation Analysis for Low Temperature Plasma Ignition of

Propane/Air, *Acta Scientiarum Naturalium Universitatis Pekinensis*, 2015, 791 (**in Chinese**).
35. B. Zhang and C. Bai, C_2H_4-O_2 Critical Energy for Direct Detonation of C_2H_4-O_2 Gas Mixture, *Explos. Shock Waves*, 2012, **32**(2), p 113-120. (**in Chinese**)
36. B. Zhang, M. Shahsavari, J. Chen, H. Wen, B. Wang, and X. Tian, The Propagation Characteristics of Particle-Laden Two-Phase Detonation Waves in Pyrolysis Mixtures of C (s)/H_2/CO/CH_4/O_2/N_2, *Aerosp. Sci. Technol.*, 2022, **130**, p 107912.
37. J. Yu, L. He, W. Ding, Y. Zhang, Y. Mao, and Y. Jiang, Comparative Study of Transient Plasma Ignition and Spark Plug Ignition Initiation Process, *Propuls. Technol.*, 2013, **34**, p 1575. (**in Chinese**)
38. 42nd AIAA M. Petrova, B. Varatharajan, and F. Williams, Theory of Propane Autoignition, Aerospace Sciences Meeting and Exhibit. 2004.
39. V.Y. Ulianitsky, D.V. Dudina, A.A. Shtertser, and I. Smurov, Computer-Controlled Detonation Spraying: Flexible Control of the Coating Chemistry and Microstructure, *Metals*, 2019, **9**, p 1244.
40. W. Krömmer, P. Heinrich, and H. Kreye, High Velocity Oxy-Fuel Flame Spraying: Past-Present-Future. *Proceedings of 8th Colloquium High Velocity Oxy-Fuel Flame Spraying*. 2009, 9-16.
41. K. Bobzin, N. Kopp, T. Warda, I. Petkovic, M. Schaefer, K.D. Landes, G. Forster, S. Zimmermann, J.L. Marques, S. Kirner, and M. Kauffeldt, Particle in-Flight and Coating Properties of Fe-Based Feedstock Materials Sprayed with Modern Thermal Spray Systems, *J. Therm. Spray Technol.*, 2013, **22**, p 363-370.
42. V. Ulianitsky, I. Batraev, D. Dudina, and I. Smurov, Enhancing the Properties of WC/Co Detonation Coatings Using Two-Component Fuels, *Surface Coat. Technol.*, 2017, **318**, p 244-249.
43. V.Y. Ul'yanitskii, A.A. Shtertser, and I.S. Batraev, Detonation of a Gas Fuel Based on Methyl Acetylene and Allene, *Combust. Explos. Shock Waves*, 2015, **51**(2), p 246-251.